Journal of Geophysical Research: Atmospheres

RESEARCH ARTICLE
10.1029/2018JD029020

The Impact of Boreal Summer ENSO Events on Tropical Lower Stratospheric Ozone

Olga V. Tweedy[1], **Darryn W. Waugh**[1,2], **William J. Randel**[3], **Marta Abalos**[4], **Luke D. Oman**[5], **and Doug E. Kinnison**[3]

[1]Department of Earth and Planetary Sciences, Johns Hopkins University, Baltimore, MD, USA, [2]School of Mathematics, University of New South Wales, Sydney, New South Wales, Australia, [3]ACOM, NCAR, Boulder, CO, USA, [4]Universidad Complutense de Madrid, Madrid, Spain, [5]GSFC, NASA, Greenbelt, MD, USA

Abstract The interannual variability of tropical lower stratosphere ozone and its connections to sea surface temperatures in the equatorial Pacific are examined using a combination of chemistry climate model simulations, satellite observations, and reanalyses. The model simulations and observations show large differences in the magnitude of interannual variability in ozone between northern tropic (NT; EQ-18° N) and southern tropic (EQ-18° S) during boreal summer but small differences in winter. The interannual variability during boreal summer is highly correlated with summer sea surface temperatures in the eastern and central Pacific Ocean and El Niño–Southern Oscillation (ENSO) events. Larger variability in NT ozone is primarily due to meridional advection, connected to the changes in the onset date and strength of the Asian summer monsoon anticyclone. The Asian summer monsoon anticyclone forms earlier in a season and tends to be stronger during cold (La Niña) events leading to more isentropic transport of ozone from the extratropics into the NT, with the reverse for warm (El Niño) events.

Key Points:
- Interannual variability in the lower stratospheric ozone is larger in the northern tropic than in the southern tropic during boreal summer
- Ozone interannual variability during boreal summer is highly correlated with boreal summer ENSO events
- Boreal summer ENSO modifies meridional advection of ozone through changes in the strength of the Asian summer monsoon anticyclone

Correspondence to:
O. V. Tweedy,
otweedy1@jhu.edu

Citation:
Tweedy, O. V., Waugh, D. W., Randel, W. J., Abalos, M., Oman, L. D., & Kinnison, D. E. (2018). The impact of boreal summer ENSO events on tropical lower stratospheric ozone. *Journal of Geophysical Research: Atmospheres*, *123*. https://doi.org/10.1029/2018JD029020

Received 17 MAY 2018
Accepted 13 AUG 2018
Accepted article online 23 AUG 2018

1. Introduction

The chemical composition of the tropical lower stratosphere (TLS) plays a key role in the climate system. Even small changes in the concentration and distribution of radiatively active gases in the TLS such as ozone (O_3) and water vapor (H_2O) significantly impact radiative forcing and thus global climate (Riese et al., 2012; Intergovernmental Panel on Climate Change, 2014). Fluctuations in stratospheric ozone affect surface ultraviolet radiation, while stratosphere-troposphere exchange of ozone impacts near-surface composition and climate. Strong spatial and temporal variability of trace gases in the lower stratosphere are mainly due to transport processes. Chemical constituents from the troposphere enter the TLS predominantly by the upwelling branch of the Brewer-Dobson circulation (BDC), while horizontal exchange of mass with extratropics is due to the meridional advection and two-way isentropic mixing by eddies (Plumb, 2006). The respective strengths of different transport processes control how fast air masses are exchanged between troposphere and stratosphere and between tropics and extratropics. In spite of the great importance of TLS composition on climate, the mechanisms that control TLS variability are not fully understood.

Earlier studies considered the TLS as being *well mixed* and the exchange of air masses with extratropics very weak (Plumb, 1996). This would result in upwelling by the BDC and local chemical sources and sinks to dominate the tracer budget in the tropical stratosphere (Randel et al., 2007). However, more recent studies revealed a dominant role of the Asian summer monsoon (ASM) anticyclone on the climatological seasonal cycle of long-lived trace gases (e.g., O_3 and CO) near the tropical tropopause (Abalos et al., 2013; Konopka et al., 2010; Ploeger et al., 2012). Furthermore, Stolarski et al. (2014) showed significant differences in tracers' seasonality between the northern (EQ-18° N) and southern (EQ-18° S) tropics (NT and ST, respectively) using satellite observations. In particular, ozone from the Microwave Limb Sounder (MLS) at 82 hPa has a larger seasonal cycle in the NT than in the ST. Tweedy et al. (2017) showed that NASA Goddard Earth Observing System Chemistry-Climate Model (GEOSCCM) and Whole Atmosphere Community Climate Model (WACCM) simulations produce NT-ST contrasts in the annual cycle of lower stratospheric ozone that are similar to the observed contrast. Furthermore, transformed Eulerian mean (TEM) tracer budget analysis from GEOSCCM and WACCM simulations shows that the ST annual cycle is dominated by upwelling, whereas in the NT, horizontal mixing during boreal summer dominates. In agreement with previous studies, Tweedy et al. (2017) attributed

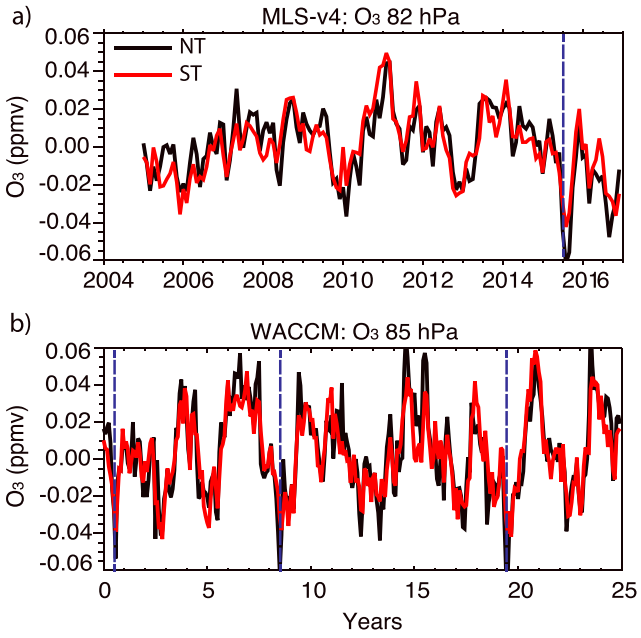

Figure 1. Deseasonalized monthly anomalies of O_3 (a) at 82 hPa from MLS and (b) at 85 hPa from WACCM simulation with coupled oceans (only 25 years are shown), averaged over the northern tropics (EQ-18° N, black) and southern tropics (EQ-18° S, red). Blue dashed lines indicate strong El Niño events during boreal summers. MLS = Microwave Limb Sounder; NT = northern tropic; ST = southern tropic; WACCM = Whole Atmosphere Community Climate Model.

the summertime increases in mixing to the ASM, which mixes in high ozone from Northern Hemisphere (NH) extratropics into the tropics.

The above studies focused on seasonal climatological composition and transport, but the TLS ozone also varies on interannual scales and El Niño–Southern Oscillation (ENSO) dominates this variability near the tropical tropopause (Calvo et al., 2010; Oman et al., 2013; Randel et al., 2009). As an example, the interannual variability of MLS O_3 at 82 hPa is shown in Figure 1a for NT and ST separately. The high correlation of NT and ST ozone anomalies strongly suggests that observed variations are driven by the uniform changes in upwelling. These anomalies are linked to variations in sea surface temperatures (SSTs) in the equatorial Pacific (ENSO events; Calvo et al., 2010; Oman et al., 2013) and are explained by changes in the strength of BDC (i.e., increase in tropical upwelling during El Niño and decrease during La Niña). However, as we will show later, this mechanism does not explain the strongest ozone anomalies in the MLS record (2004–present) in the NT during 2015 boreal summer (the only strong El Niño event during NH summer in the MLS record). Similar variability with larger NT than ST ozone anomalies during 2015 boreal summer are also found at 100 hPa (the vertical level nearest to the tropical tropopause). A short record of MLS ozone does not allow determining if this difference in NT and ST ozone is due to random noise, instrument errors, or some real physical mechanisms. However, longer time series of ozone are available from model simulations (Figure 1b, blue dashed lines), and these show similar ozone anomalies that, as in 2015, occur during boreal summers with strong positive SST anomalies in the equatorial Pacific.

It is possible that ENSO modulates advective transport (either vertical or horizontal) and/or mixing by eddies in the tropics differently during the boreal summer than winter. So far, observational investigations of ENSO-related variability in mixing, focusing on a range of different altitudes, have shown somewhat differing results. Based on the effective diffusivity calculations and ERA-15 reanalysis, Scott et al. (2003) observed weaker mixing at 350 K during strong El Niño years but their results showed a strong sensitivity to the change of the reanalysis data set. Garny et al. (2007) examined the interannual variability of mixing based on The National Centers for Atmospheric Prediction and the National Center for Atmospheric Research reanalysis over the period 1979–2005 on three isentropic levels (450, 550, and 650 K) in the stratosphere and found no significant effect of ENSO. Abalos et al. (2016) showed that ENSO modifies isentropic mixing, which could impact transport of tracers and contribute to NT/ST differences. Recently, Yan et al. (2018) analyzed the ENSO influence on the ASM anticyclone with major focus on how the ENSO winter signal propagates into the following seasons. Using satellite (MLS), in situ (Southern Hemisphere ADditional OZonesondes) observations and model simulations (Chemical Lagrangian Model of the Stratosphere) of ozone, they showed weaker ozone transport into the tropics during the onset of the ASM after boreal winter El Niño events, but the difference between El Niño and La Niña composites becomes insignificant in the summer. Yan et al. (2018) also suggested that El Nino-related anomalies may be reinforced through late boreal summer and fall if the El Niño conditions last until next winter. However, they showed it only for three cases between 1979 and 2015.

The above studies focused on cold-season (December–February) SST anomalies in the equatorial Pacific because ENSO usually peaks during boreal winters. However, there are also ENSO events that are strong or moderately strong during boreal spring and summer (e.g., 2015/2016 El Niño) and some peak during summer (e.g., the 1987/1988 El Niño). As we will show later in this study, analysis of WACCM shows a strong correlation of ozone with SSTs leading ozone anomalies just by 1 month. This demands evaluation of the role of ENSO events during the NH warm seasons (late boreal spring and summer) on interannual variability of ozone in the TLS, an issue that has received little attention in literature.

In this study we examine O_3 transport from model simulations over interannual time scales and compare them to observations and reanalysis. In particular, we explore how SSTs in the tropical Pacific modify transport processes and thus distribution of ozone in this region. In the next section we briefly describe the model, data,

and methodology. ENSO-related interannual variability and the influence of ENSO on ozone seasonality are examined in section 3.1 In sections 3.2 and 3.3, we evaluate ozone transport and explore the causes of ozone variability in the TLS. Discussion of results and conclusions are in section 4.

2. Model, Data, and Methodology

2.1. Model Simulations and Data

In this study we examine the response of the TLS ozone to boreal summer ENSO in version 4 of the WACCM (Garcia et al., 2007, 2017; Marsh et al., 2013). WACCM includes an interactive atmospheric chemistry package and is coupled to the ocean, land, and sea ice components of the Community Earth System Model version 1. This model self-consistently develop SST anomalies, teleconnections between ocean and atmosphere and allows us to examine the stratospheric response to a larger number of ENSO events than have occurred in the historical record. The WACCM simulation has horizontal resolution of 1.9° latitude by 2.5° longitude, 66 vertical levels (from surface to near 140 km) and vertical resolution around 1.2–1.4 km near the tropopause and in the lower stratosphere. We analyze a simulation from 1960 to 2100 where greenhouse gases, tropospheric ozone precursors, and aerosol emissions follow the Representative Concentration Pathway 6.0 and ozone-depleting substances follow the World Meteorological Organization A1 scenario (Meinshausen et al., 2011). Abalos et al. (2013) showed that the simulated annual cycle in ozone and temperature in WACCM agrees well with satellite observations in the TLS. Furthermore, Tweedy et al. (2017) showed that WACCM simulations capture the observed larger amplitude of the seasonal cycle in the lower stratospheric ozone in the NT than in the ST, which indicates that it also captures the interhemispheric differences in TLS transport processes. We have confirmed that this also holds for the WACCM simulation considered here.

The ozone of the coupled model simulation is compared with measurements from the MLS on board the Aura satellite. The MLS data provide horizontal, vertical, and temporal coverage suitable for examining seasonal changes in O_3, while the continuous record over 13 years allows characterizing interannual variations. We use Version 4.2 MLS level 2 data at 100 hPa to construct a monthly mean data set for January 2005 through 2017. The data are binned into 2.5° latitude by 5° longitude grid, using the recommended quality and convergence thresholds (Livesey et al., 2015).

Meteorological fields are from Modern-Era Retrospective analysis for Research and Applications, version 2 (MERRA-2). MERRA-2 is the latest atmospheric reanalysis of the modern satellite era produced by NASA's Global Modeling and Assimilation Office and is available for 37 years (1980–present; Bosilovich et al., 2015). A detailed overview of MERRA-2, including a description of the data assimilation system and various measures of performance can be found in Gelaro et al. (2017).

We use SST data from the Met Office Hadley Centre's sea ice and Sea Surface Temperature (HadISST) data set for the statistical validation of a free-running climate model where SSTs are not prescribed. The HadISST data set combines monthly mean fields of SST and sea ice concentration on a 1-degree latitude-longitude grid from 1850 to date. In this study we use SST fields from 1980 to 2017. For a detailed description of the data set and its production process, see Rayner et al. (2003).

2.2. Methodology

In this study we primarily focus on ozone that is near the tropical tropopause. At this level the ASM impact on ozone distribution during boreal summer is expected to be the strongest. As the tropopause is higher in WACCM than in observations (shown in Abalos et al., 2013), we examine ozone at 85 hPa in the model and at 100 hPa in observations. For both WACCM and observations we follow Stolarski et al. (2014) and Tweedy et al. (2017) and calculate NT and ST ozone as area averages between EQ-18° N and EQ-18° S.

ENSO events in observations are identified based on SST anomalies averaged over the Niño34 region (5° N to 5° S, from 170° W to 120° W) that are above a specified threshold. SST fields are not available for WACCM simulation, and surface air temperatures (SATs) are used instead to calculate the ENSO index. Although SATs and SSTs are not exactly the same, their variability is very similar (i.e., the explained variance between SSTs and SATs from WACCM simulations with prescribed SSTs is 99% [not shown]). SST and SAT anomalies are calculated by removing long-term linear trend and seasonal cycle.

In this study, we distinguish between boreal winter (cold-season) and summer (warm-season) events (see Figure 2 and section 3.1 for more details). We identify El Niño (La Niña) conditions when Nino34 index is larger (smaller) than +0.5 K (−0.5 K). However, our main focus is on strong warm-season ENSO events, which are

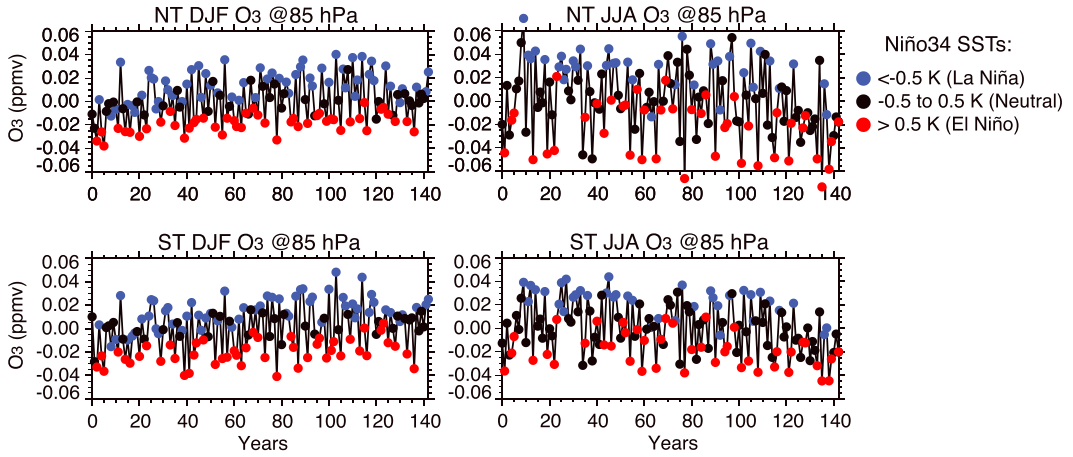

Figure 2. Deseasonalized ozone anomalies at 85 hPa from the Whole Atmosphere Community Climate Model simulation averaged over the NT (top) and ST (bottom) and over the winter (DJF) and summer (JJA) months. Colored symbols are Niño34 SST anomalies larger/smaller than +0.5 K/−0.5 K (red and blue, respectively) 1 month prior to ozone values. DJF = December–February; JJA = June–August; NT = northern tropic; ST = southern tropic; SST = sea surface temperature.

identified when May and June (MJ) SAT anomalies in the Niño34 region exceed ±1 K in WACCM and ±0.8 K in observations. A smaller threshold for the observations was chosen to select a larger number of ENSO events for our analysis (since observational record is much shorter with fewer ENSO events during boreal summer).

In section 3.2 a TEM tracer budget analysis (Equation 9.4.13 in Andrews et al., 1987) is used to quantify the relative role of different transport processes and chemical production and loss in causing changes in ozone tendency, that is,

$$\frac{\partial \overline{O_3}}{\partial t} = -\overline{v^*}\frac{\partial \overline{O_3}}{\partial y} - \overline{w^*}\frac{\partial \overline{O_3}}{\partial z} + \frac{1}{\cos\phi}e^{z/H}\frac{\partial (M_y \cos\phi)}{\partial y} + P - L, \quad (1)$$

where $(\overline{v^*}, \overline{w^*})$ are the meridional and vertical components of the residual circulation, $P - L$ is the chemical production minus loss rate, and M_y is the horizontal component of eddy transport vector, calculated as $M_y \equiv -e^{-z/H}(\overline{v'O_3'} - \frac{\partial \overline{O_3}}{\partial z}\overline{v'T'}/S)$. The small vertical eddy term is neglected because not all fields were available as daily outputs for these runs. The first two terms on the right-hand side correspond to vertical and horizontal advection, which reduce trace gas concentration in the tropics when the residual circulation and ozone gradients are both positive. In other words, increased upwelling transports ozone-poor air from the tropopause to the TLS while poleward (positive in the NH) meridional transport moves low in ozone tropical air into the northern subtropics.

3. Results

3.1. Hemispheric Asymmetries in the Tropical Ozone Interannual Variability

Previous studies by Stolarski et al. (2014) and Tweedy et al. (2017) showed that annual cycle amplitude in ozone is different between NT and ST due to hemispheric differences in transport processes; however, interannual variability in the NT and ST ozone in the TLS was not examined. To explore this interannual variability we examine deseasonalized ozone anomalies from WACCM simulation for NT and ST separately and also distinguish between boreal summer (June–August [JJA]) and winter (December–February [DJF]) months. Figure 2 shows that the NT ozone anomalies during JJA are larger than corresponding anomalies averaged over the ST as well as both NT and ST ozone anomalies during DJF. This is suggestive of different mechanisms controlling NH summertime ozone variability in the NT.

The ozone anomalies shown in Figure 2 have a strong relationship with SATs in the equatorial Pacific (Niño34 region in particular). Years when the SAT anomalies in the Niño34 region are larger than +0.5 K (El Niño events) and smaller than −0.5 K (La Niña events) are respectively shown by red and blue dots. There is a distinct separation of colors for both NT and ST ozone and during both seasons. Blue dots (cold La Niña events) are collocated with high O_3 anomalies and red dots (warm El Niño events) with low O_3 anomalies, demonstrating a strong negative correlation between ozone and Niño34 index.

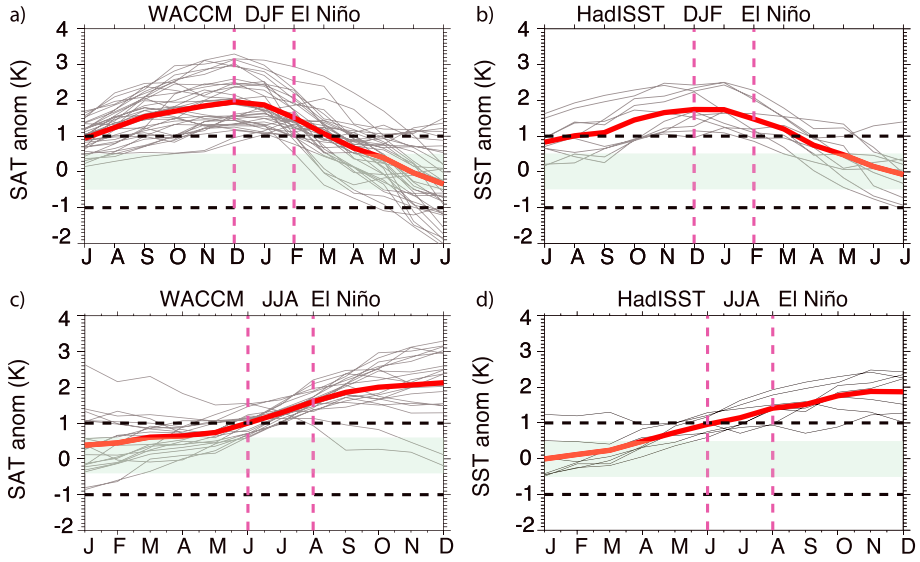

Figure 3. Seasonal evolution of detrended and deseasonalized SAT and SST anomalies over the Niño34 region (5° N to 5° S; 120° W to 170° W) from the WACCM simulation and HadISST data set averaged for (a, b) DJF El Niño events and (c, d) JJA El Niño events. Black curves show all years in WACCM or observations when (a, b) the DJF SATs/SSTs anomalies are greater than +1 K or (c, d) when JJA anomalies are greater than 1 K for WACCM or 0.8 K for HadISST. Thick red contour is an average of all events. Green shading highlights ENSO neutral conditions (between −0.5 and +0.5 K) with horizontal dashed lines indicating boundaries of strong ENSO events (±1K). DJF = December–February; JJA = June–August; HadISST = Hadley Centre's sea ice and Sea Surface Temperature; SAT = surface air temperature; SST = sea surface temperature; WACCM = Whole Atmosphere Community Climate Model.

To evaluate how realistic ENSO events are in the model, we compare seasonal evolution (i.e., buildup and decay) of El Niño events from WACCM and the HadISST data set, for DJF (Figures 3a and 3b) and JJA events (Figures 3c and 3d). This shows that WACCM generates realistic DJF and JJA El Niño events, with seasonal evolution in a good agreement with observations. In both the model and observations, the majority of DJF El Niño events start to develop during late spring and early summer, peak during boreal winter and rapidly decay after DJF with SST anomalies becoming neutral during late boreal spring and summer. In contrast, the majority of JJA El Niño events (~67% of all cases in WACCM and all except one El Niño in observations) are developing El Niño that will become mature during following winter. In addition there are also El Niño events that do not decay or decay slowly after boreal winter and remain strong throughout following spring and summer, known in literature as *no-decay* (Chowdary et al., 2016) or *long-lasting* (Brönnimann et al., 2004; Li et al., 2018; Yan et al., 2018), El Niño events, which are also included in our analysis. These are less common than developing JJA El Niño events, with ~33% of WACCM and only one observed JJA El Niño being a long-lasting event. Long-lasting El Niño events are more common during late spring and early summer contributing to nearly half of all cases. While El Niño events during the boreal summer (both developing and long-lasting) are weaker and less frequent than during boreal winter, in both WACCM and observations, there is still a large number of years with summer SST anomalies exceeding +1 K. Similar results but opposite in magnitude hold for La Niña events (not shown).

Other studies have also shown that WACCM reproduces the key features of SST anomalies associated with ENSO (Jian & Rong-Cai, 2014; Kim & Yu, 2012; Marsh et al., 2013; Yang & Giese, 2013). Marsh et al. (2013) showed that WACCM reproduces well the periodicity in the Nino34 index but overestimates the amplitude of ENSO events, as can also be seen in Figures 3a and 3b. Jian and Rong-Cai (2014) evaluated statistical characteristics of ENSO events from 24 Coupled Model Intercomparison Project Phase 5 models and showed that WACCM can successfully reproduce the relatively higher frequency of cold-season-matured ENSO events (peak phase in the boreal winter, DJF) than warm-season-matured events (peak phase in the boreal summer, JJA). In their study, the composite intensity of El Niño and La Niña for WACCM is comparable to ERSST data set and overall WACCM performs above average compared to other Coupled Model Intercomparison Project Phase 5 models.

As the observed ENSO tends to be strongest during boreal winters, previous studies have focused primarily on cold-season-matured ENSO events and their influence on TLS composition during boreal winter and

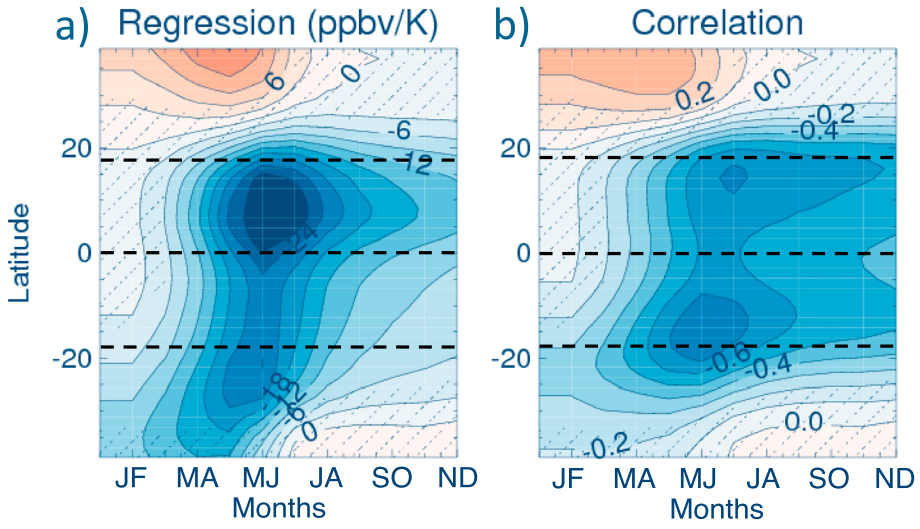

Figure 4. (a) Regression (in ppbv/K) and (b) correlation of June–August deseasonalized ozone anomalies from the Whole Atmosphere Community Climate Model simulation at 85 hPa with 2-month-running average of Niño34 index. Dashed horizontal lines indicate 18° N, equator, and 18° S. Areas without hatching indicate regions where regression coefficients are significant above three standard deviations.

spring. However, Figure 2 shows that simulated ozone anomalies in the NT are largest during boreal summer. To isolate ozone variability during summer and the strength of the relationship of this variability with SSTs, we examine the regression and correlation coefficients of JJA ozone anomalies with the Niño34 index for different months, see Figures 4a and 4b. This shows large (negative) regression and correlation coefficients in tropical ozone with summer SAT anomalies (i.e., correlations less than −0.6 for MJ) but low values for SAT anomalies from the preceding winter (correlations near 0 for months January and February). Thus, ozone anomalies during JJA have the strongest sensitivity to the SST changes during MJ, and the sensitivity rapidly decreases toward the winter indicating weak influence of boreal winter ENSO on summertime ozone.

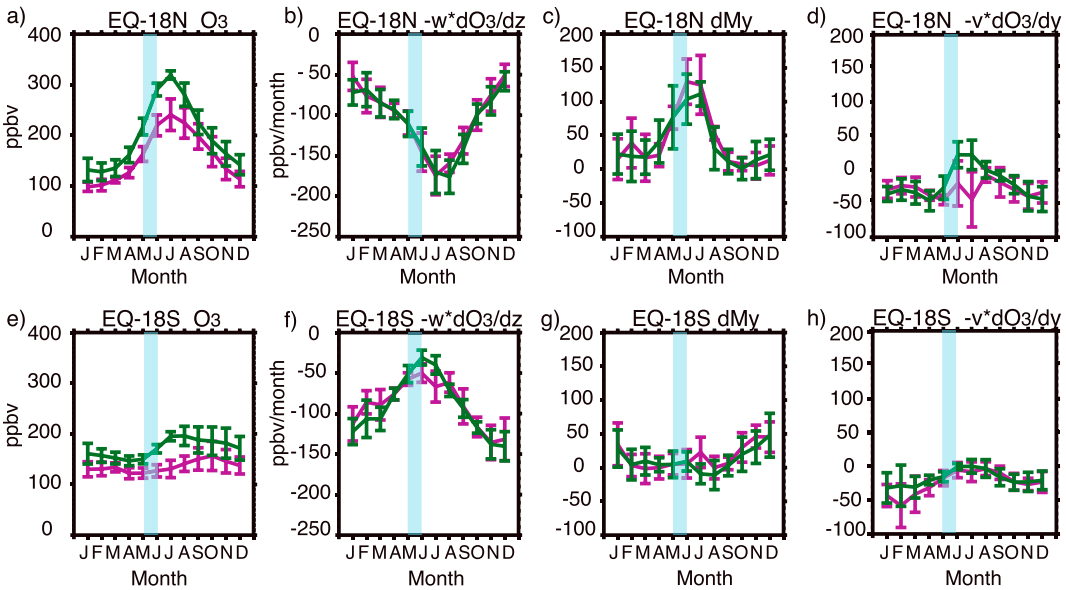

Figure 5. El Niño (purple) and La Niño (green) composites of (a) ozone annual cycle, (b) vertical advection, (c) horizontal mixing, and (d) meridional advection averaged over the NT (EQ-18° N, top) and ST (EQ-18° S, bottom) from the Whole Atmosphere Community Climate Model simulation. Composites are based on Niño34 index during May and June indicated by blue shading. Vertical bars show ±1 standard deviation away from the mean. Units are in parts per billion by volume per month.

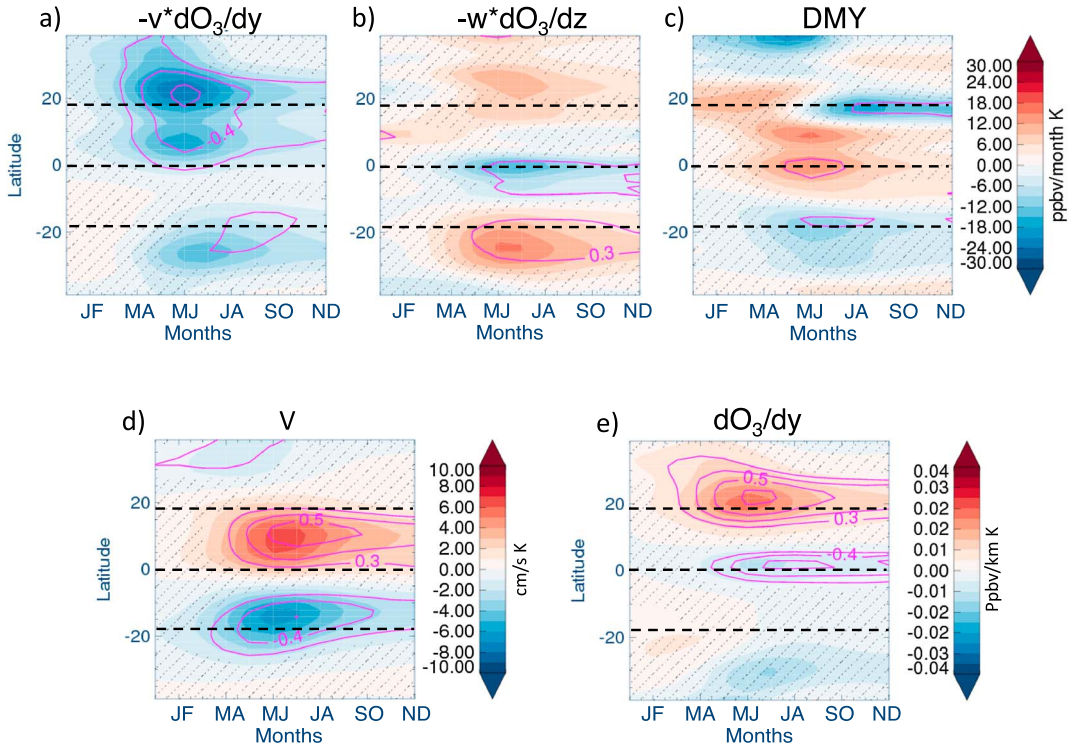

Figure 6. Regression (filled contours) and correlation (magenta) of (a) meridional advection, (b) upwelling, (c) horizontal mixing, and (d, e) meridional velocity and horizontal ozone gradients during JJA at 85 hPa with 2-month-running average of Niño34 surface air temperature anomalies. Areas without hatching indicate regions where regression coefficients are significant above three standard deviations.

The decrease in tropical ozone during boreal summer El Niño events has a large impact on ozone annual cycle amplitude. Figures 5a and 5e show El Niño and La Niña composites of ozone seasonality based on Niño34 index during MJ for NT and ST, respectively. The annual cycle amplitude in ozone is larger during La Niña (green) than El Niño (purple). Furthermore, in agreement with Stolarski et al. (2014) and Tweedy et al. (2017), ozone seasonality is larger in the NT than in the ST for both ENSO composites. The differences between ENSO composites are largest during JJ in the NT and JA in the ST.

3.2. ENSO-Related Variability in Transport

The local change in ozone concentration due to transport processes and chemical sources and sinks are quantified by the TEM continuity equation (equation (1). ENSO composites of the ozone seasonal cycle and its major transport terms (upwelling, isentropic mixing, and meridional advection) are shown in Figure 5 for the NT (panels b–d) and ST (panels f–h). In the NT, there is a clear difference for ozone in El Niño and La Niña composites during summer, primarily attributable to differences in meridional advection during JJ. During this period there is a positive tendency during La Niña but a negative tendency during El Niño. Isentropic mixing is stronger during El Niño than during La Niña in JJ, but the difference between two composites is much smaller than for meridional advection and one-standard deviation bars overlap. In the ST, the differences in the JA ozone are mostly due to differences in upwelling during JJ with error bars only slightly overlapping between two composites. Note that enhanced mixing during boreal summer in the NT is a major contributor to larger climatological seasonal cycle amplitude in the NT than in the ST ozone; however, interannual variability of the NT summertime ozone is dominated by variations in meridional advection modulated by smaller differences in isentropic mixing.

The above conclusions are also supported by regression and correlation analysis of JJA TEM transport terms at 85 hPa with the ENSO index (Figures 6a–6c). In agreement with Figure 5, meridional advection is a dominant term in the NT, with enhanced statistically significant negative sensitivity and correlation with Niño34 index during late spring and early summer. Summertime isentropic mixing has nonnegligible positive sensitivities in the NT with Niño34 index, but their correlation coefficients are smaller than 0.3 almost everywhere. Vertical

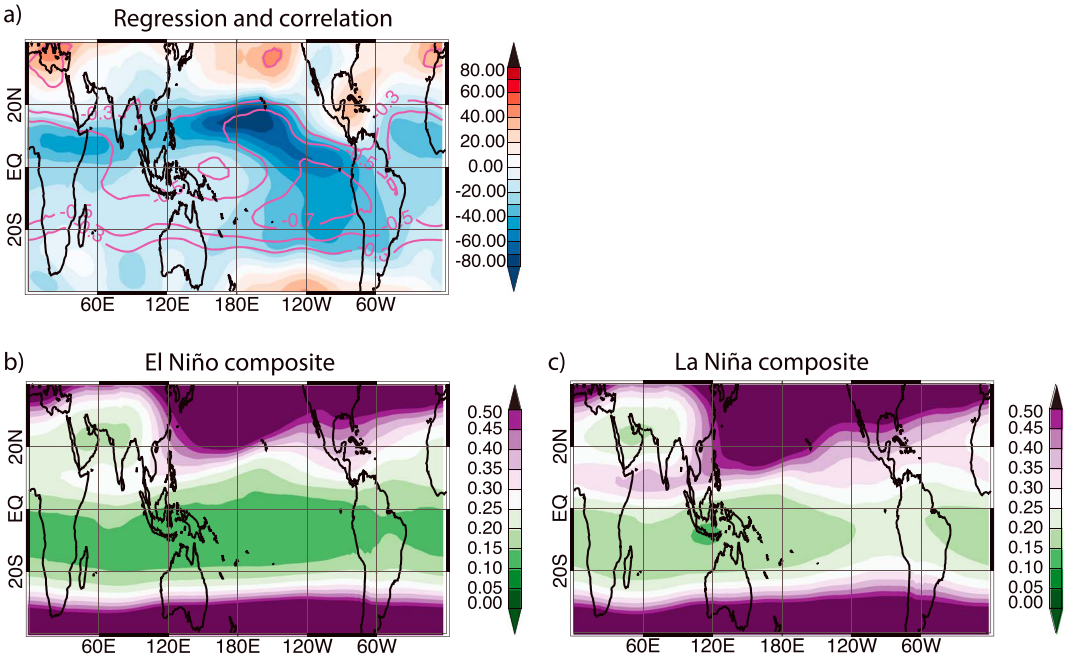

Figure 7. (a) Regression (color) and correlation (magenta) of June–August deseasonalized ozone anomalies with May and June Niño34 index from the Whole Atmosphere Community Climate Model simulation. Correlation coefficients that are between −0.3 and 0.3 are not shown. (b) El Niño and (c) La Niño composites of ozone during June–August based on Niño34 index in May and June. Units are in parts per billion by volume per Kelvin in (a) and parts per million by volume in (b) and (c).

advection in the NT has negligible sensitivities and very weak correlation with Niño34 index during the summer. However, this term has a strong sensitivity to the changes in summertime SAT anomalies in the ST with correlation coefficients below −0.3. These results are consistent with larger annual cycle amplitude during MJ La Niña than El Niño. Thus, interannual variability in the NT summertime ozone is dominated by changes in meridional advection, while ENSO-related changes in the upwelling dominate the ST ozone variability.

The pronounced negative peak in the meridional advection in the NT is due to two factors. First, meridional velocities (v^* and also v in general) are more positive during boreal summer El Niño than La Niña events (Figure 6d), indicating weaker inflow of subtropical air into the NT during El Niño. Second, the maximum in ozone meridional gradient during boreal summer is located further northward in the NT during El Niño (Figure 6e). Both factors contribute to the reduction (increase) in the NT ozone during warm-season El Niño (La Niña) and, therefore, a smaller (larger) annual cycle amplitude.

Not all terms in the TEM continuity equation are shown in Figures 5 and 6. The net P-L is nearly identical between El Niño and La Niña cases and therefore not shown. Vertical eddy mixing terms are not available for this simulation but assumed to be a smaller contribution in the TLS (Abalos et al., 2013; Tweedy et al., 2017). Given the relatively small differences in ozone between El Niño and La Niña cases, absence of this term provides additional uncertainty in our calculations. Additional errors also could be due to use of daily data instead of smaller time steps (6-hourly or 4-hourly) to calculate horizontal eddy term. Nevertheless, the TEM analysis provides valuable insights into the nature of processes that cause ozone changes in the TLS. The boreal summer ENSO alters the meridional advection in the northern tropics and subtropics leading to larger variability in the NT summertime ozone, while in the ST the ozone variability is dominated by changes in upwelling related to ENSO.

3.3. Zonal Variations: Role of the ASM Anticyclone

The analysis in the previous sections has focused on zonally averaged characteristics of ozone and transport. However, the NH summertime ozone transport in the TLS has large zonal variations that need to be considered. A major cause of these zonal variations is the ASM anticyclone. For instance, two-dimensional meridional advection from TEM analyses translates into the transport in the outer flanks of the ASM anticyclone, mainly

Table 1
Niño3.4 Index Larger and Smaller Than ±0.8 K Since 1980 for May to August from HadISST Data Set

Year	May	June	July	August
1982	0.65	0.92	0.64	0.93
1983	1.12	0.62	−0.11	−0.13
1984	−0.60	−0.90	−0.40	−0.44
1985	−0.90	−0.76	−0.61	−0.49
1987	0.91	1.24	1.34	1.48
1988	−1.05	−1.46	−1.54	−1.44
1989	−0.80	−0.64	−0.47	−0.58
1992	1.27	0.53	0.27	−0.15
1993	0.93	0.64	0.33	0.16
1997	0.87	1.15	1.60	1.94
1998	0.68	−0.39	−0.73	−0.83
1999	−0.87	−0.95	−0.84	−0.98
2000	−0.80	−0.75	−0.57	−0.36
2010	−0.15	−0.62	−0.89	−1.33
2015	1.04	1.28	1.56	1.87
EL/LA	6/5	4/3	3/3	4/4

Note. Warm sea surface temperature anomalies (El Niño events) are in red, cold anomalies are in blue (La Niña events), and values that are between −0.8 and 0.8 K are in black. Last row indicates total number of El Niño (EL) and La Niña (LA) for corresponding month. HadISST = Hadley Centre's sea ice and Sea Surface Temperature.

from extratropics into the tropics. We now examine ENSO-related differences in the horizontal structure of ozone and winds.

Figure 7a shows a map of the regression (shaded) and correlation (contours) coefficient of JJA ozone anomalies at 85 hPa with MJ Niño34 SAT anomalies. A strong negative correlation with the Niño34 index throughout the tropics (18° N to 18° S) indicates that overall ozone is smaller following El Niño than La Niña (consistent with Figures 5a and 5e). However, the regression coefficients are larger (more negative) in the NT than in the ST with the largest magnitude above the tropical Pacific Ocean (120° E to 120° W) and Africa-northern Indian Ocean sector (20° E to 70° E).

Analysis of ENSO composites for JJA ozone shows a stronger inflow of ozone rich air deep into the NT during La Niña than El Niño events (compare Figures 7b and 7c). This differs from Yan et al. (2018) who have shown a stronger in-mixing of ozone into the NT during La Niña than El Niño events during April-June (AMJ) but almost no difference in ozone fields during boreal summer (JJA) when compositing on wintertime (DJF) ENSO events (see their Figures 7 and 8). See section 4 for further comparisons with Yan et al. (2018).

The geographical distribution of ENSO-related anomalies in ozone fields strongly suggests an important role of the ASM anticyclone in ozone transport. As stated in section 1, the ASM can impact transport of chemical constituents by either meridional advection or isentropic mixing. The TEM analysis indicates that meridional advection is the dominant cause of differences in ozone in the NT between El Niño and La Niña cases during boreal summer. To examine this further we analyze composites of the stream function for warm-season El Niño (Figure 8a) and La Niña (Figure 8b) events. We composite 85-hPa stream function based on Niño34 index for May, June, and July separately. In May, the ASM anticyclone during El Niño is not fully developed but during La Niña the anticyclone is already formed as indicated by circular enclosed contours and positive values of stream function above Asia. The anticyclone is fully formed in June but remains much weaker during El Niño than La Niña years. In July, the ASM is still weaker during El Niño but the difference between two composites is smaller. These results are in agreement with previous studies that examined the impact of warm-season ENSO on the onset date and strength of the ASM (Ju & Slingo, 1995; Webster & Yang, 1992). Webster and Yang (1992) show a variation of 25 days between the weak, late monsoon of 1987 (strong El Niño conditions) compared with the

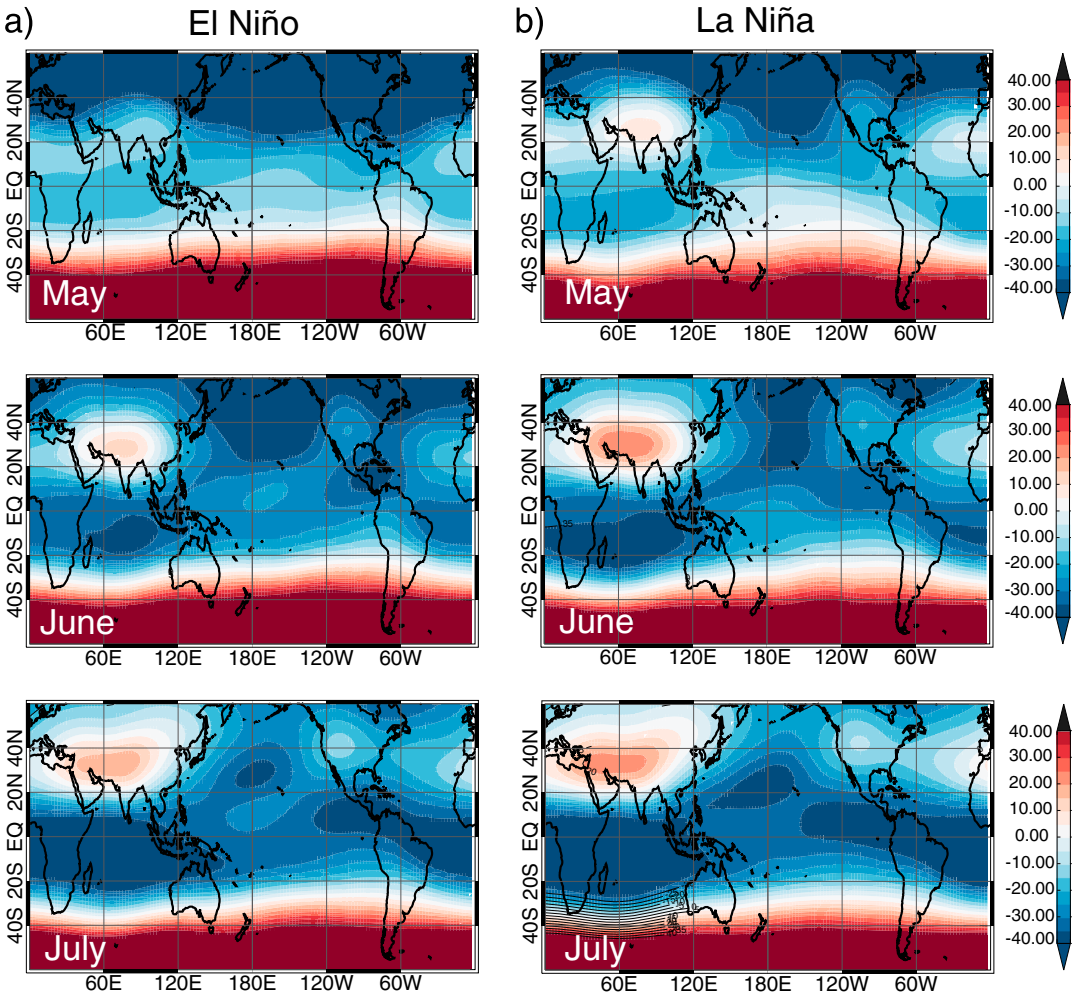

Figure 8. (a) El Niño and (b) La Niña composites of stream function at 85 hPa from Whole Atmosphere Community Climate Model based on Niño34 index (±1 K) for the same month during May (top), June (middle), and July (bottom). Units are in 10^6 m^2/s.

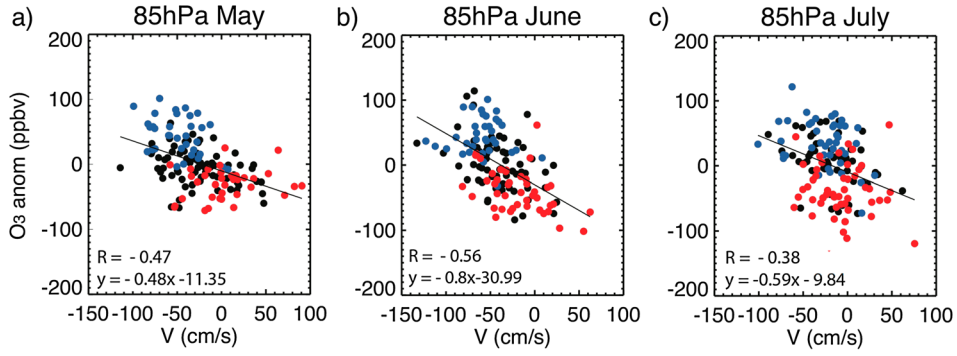

Figure 9. Relationship between 85-hPa ozone anomalies and meridional velocity (*v*) for 144 years in Whole Atmosphere Community Climate Model simulation in (a) May, (b) June, and (c) July. O_3 and *v* are averaged over the northern Pacific Ocean (EQ-18° N and 120° E to 120° W). Years with sea surface temperature anomalies greater (smaller) than +0.5 K (−0.5 K) in Niño34 region are shown in red (blue). Black line shows the linear regression between ozone and *v*, with Pearson linear correlation coefficient (*R*) and equation of linear regression line in the bottom left corner of each panel.

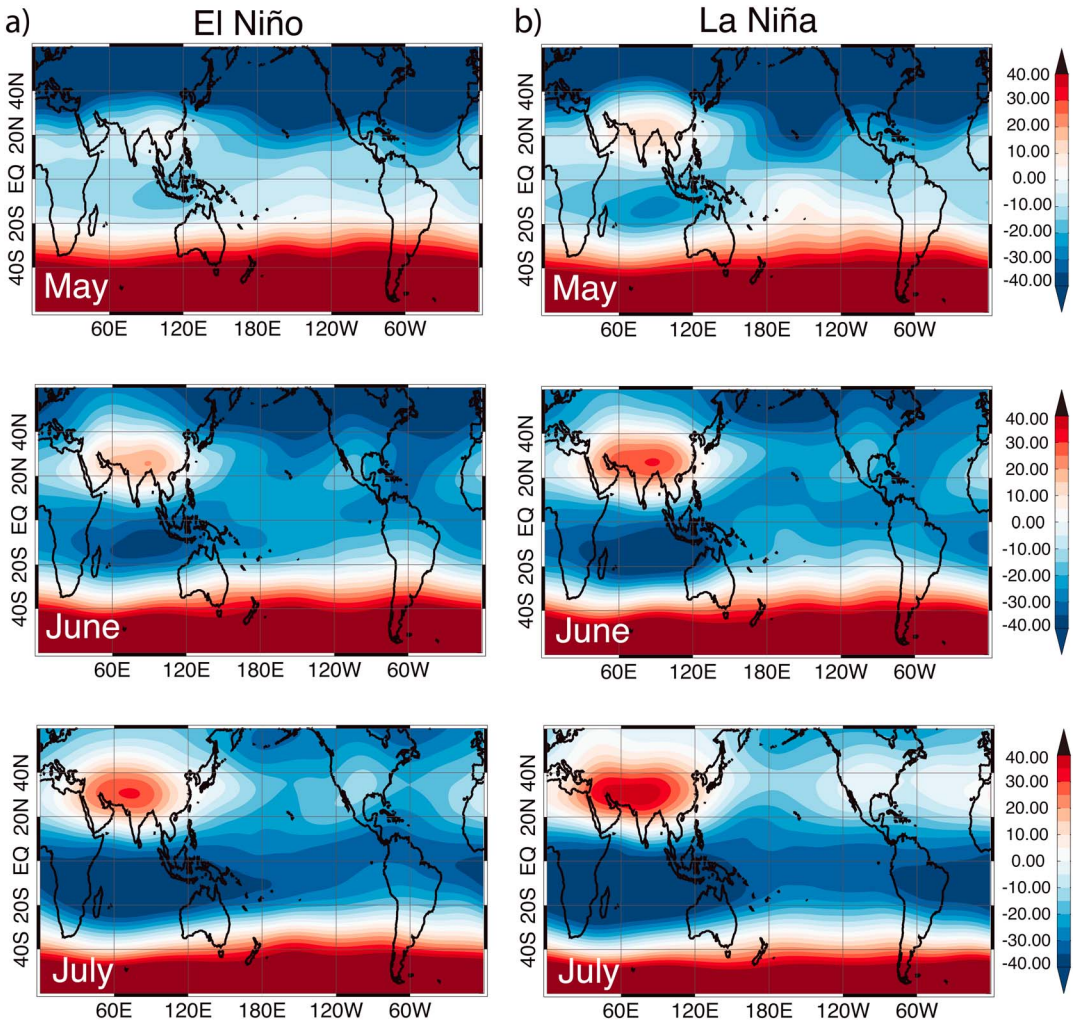

Figure 10. The same as in Figure 8 only from Modern-Era Retrospective analysis for Research and Applications, version 2 at 100 hPa. Composites are based on Niño34 index (±0.8 K) for the same month. Number of cases in the composites are 6 in May, 4 in June, and 3 in July.

strong, early monsoon of 1986 and also suggested that the biggest differences in the strength of the monsoon flow occur during the onset (May and early June) and the mature stages of the monsoon development (June and July).

The equatorward meridional winds in the NT Pacific (120° E to 120° W) are weaker (stronger) during El Niño (La Niña) in May and June leading to lower (higher) ozone in this region (also seen as stronger negative regression between 120° E and 120° W in Figure 7a). This negative relationship between the simulated *v* and O_3 anomalies at 85 hPa is demonstrated in Figure 9 from May to July, showing more O_3 when equatorward flow is stronger. This relationship is strongest during June. During La Niña years (blue symbols), ozone anomalies and *v* are overall larger than during El Niño years (red symbols). This is consistent with zonal mean TEM analysis showing stronger meridional advective transport of ozone into the NT during La Niña than during El Niño.

Testing the above results in observations is difficult given the short data record for MERRA-2. The number of strong El Niño (La Niña) events that are larger (smaller) than +0.8 K (−0.8 K) since 1980 in MERRA-2 reanalysis is 6 (5) in May, 4 (3) in June, and only 3 (3) in July; see Table 1. However, despite the limited number of cases with strong ENSO events during late boreal spring and summer, the El Niño and La Niña composites of the stream function calculated from MERRA-2 winds at 100 hPa (Figure 10) agree well with WACCM results (Figure 8) and conclusions made above. The ASM anticyclone in MERRA-2 forms later and is weaker during boreal summer El Niño events.

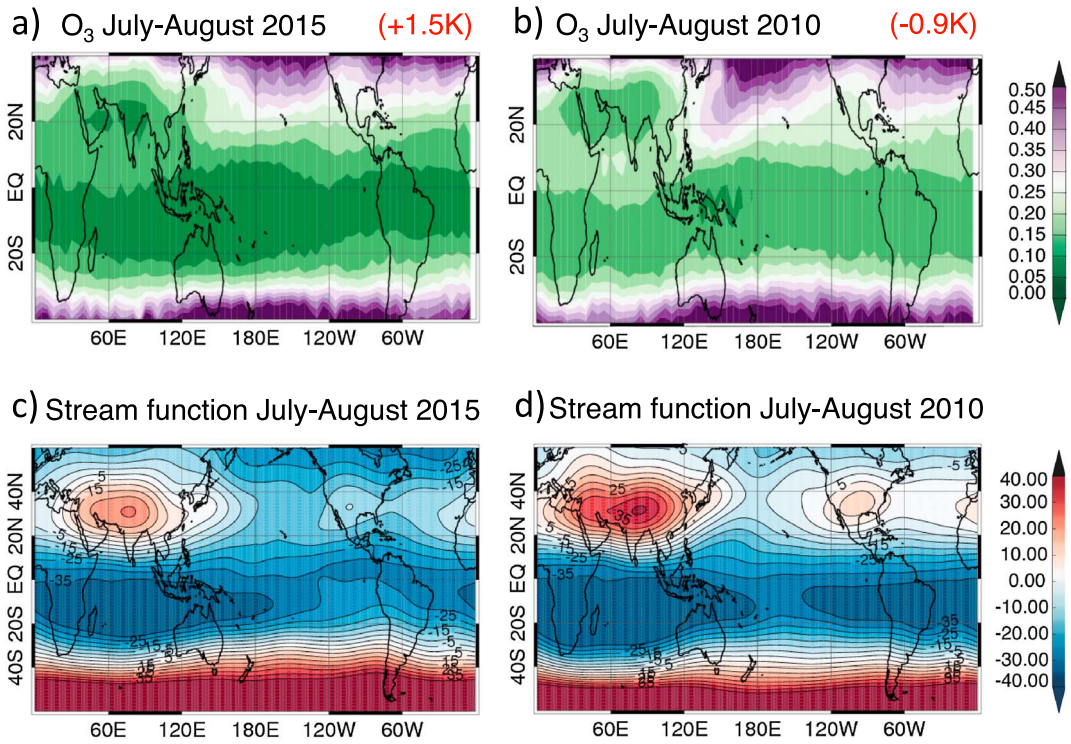

Figure 11. (a, b) Ozone from Microwave Limb Sounder (in ppmv) and (c, d) stream function from Modern-Era Retrospective analysis for Research and Applications, version 2 (in 10^6 m^2/s) during July–August 2015 (El Niño) and 2010 (La Niña). Niño34 index for July–August in 2015 and 2010 are shown in red.

Examination of the interannual variability in ozone and ozone transport using observations is even more complicated as there is an even shorter MLS data record. There has been only one strong El Niño (2015) and one La Niña (2010) event occurring during boreal summer since 2004. In 2015, the Niño34 SST anomalies were already above +1 K during late spring and they reached +1.8 K by August. In 2010, Niño34 SST anomalies were −0.6 K in June, −0.9 K in July, and −1.3 K in August. Therefore, in Figures 11a and 11b we show JJA averaged ozone from MLS at 100 hPa during 2015 (El Niño) and 2010 (La Niña), respectively. Ozone values in 2015 are smaller on average than in 2010 throughout most of the tropics. There is also stronger ozone inflow into the NT during 2010 at the Eastern flank of the anticyclone. Differences in the NT ozone between El Niño and La Niña cases are in good agreement with the strength of the monsoon anticyclone (e.g., in 2010 monsoonal flow is stronger than in 2015, see Figures 11c and 11d)

4. Discussion and Conclusions

In this study a coupled ocean chemistry climate model and observations have been used to investigate the influence of boreal summer ENSO events on the ozone in the TLS. We have shown that ozone interannual variability is larger in magnitude in the NT during the boreal summer than during the winter and also larger than in the ST during both seasons. JJA ozone anomalies are strongly correlated with SSTs in the central equatorial Pacific (Niño34 region), and correlation is strongest when O_3 anomalies lag Niño34 index by 1 month.

A TEM budget analysis of the CCM allowed us to assess the role of different transport processes on the ozone distribution. The seasonal cycle amplitude in ozone is larger in the NT than in the ST for all years (El Niño, La Niña and ENSO neutral years) due to enhanced summertime mixing in the NT associated with ASM anticyclone (Tweedy et al., 2017). However, boreal summer ENSO events alter the meridional advection in the northern subtropics leading to larger variability in the NT summertime ozone, while in the ST ozone variability is dominated by changes in upwelling related to ENSO (just like during the winter [Calvo et al., 2010]). These lead to larger annual cycle amplitude during boreal summer La Niña and smaller amplitude during boreal summer El Niño events in both ST and NT.

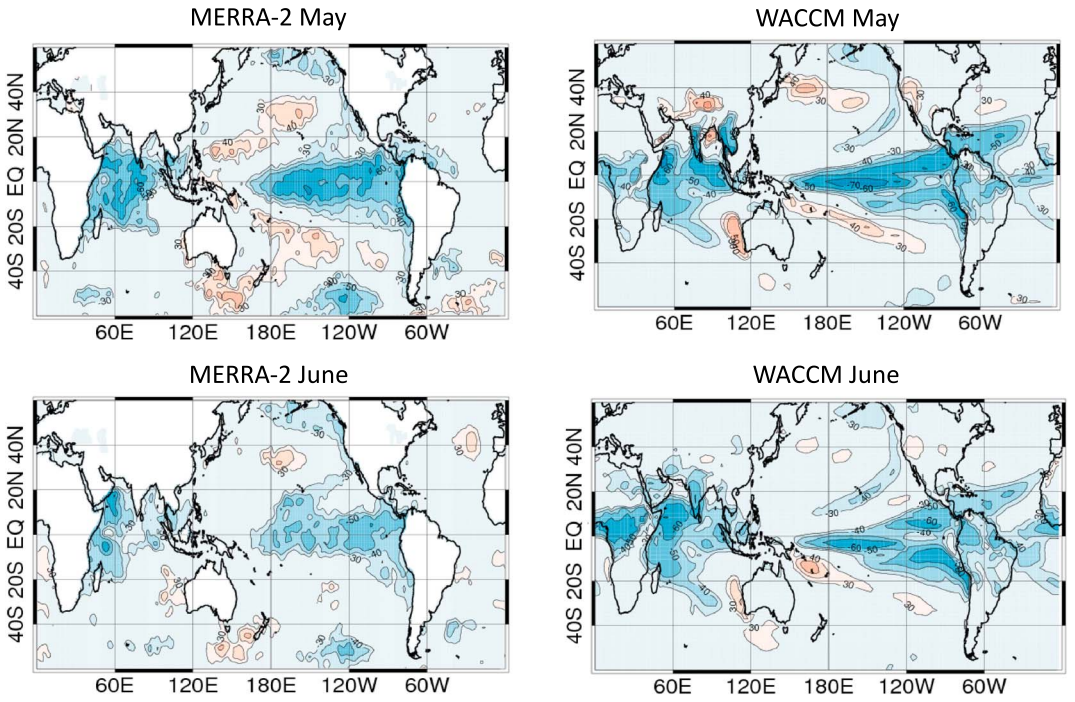

Figure 12. Correlation of the 100-hPa stream function averaged over anticyclone region (May: 10° N to 30° N and 60° E to 120° E; June: 20° N to 40° N and 20° E to 100° E) from WACCM/MERRA-2 with sea surface temperature/surface air temperature anomalies from WACCM/HadISST for May and June. Correlation coefficients are multiplied by 100, and values that are between −30 and 30 are not shown. HadISST = Hadley Centre's sea ice and Sea Surface Temperature; MERRA-2 = Modern-Era Retrospective analysis for Research and Applications, version 2; WACCM = Whole Atmosphere Community Climate Model.

The changes in the meridional advection during boreal summer ENSO are related to changes in the onset date and strength of the ASM anticyclone. The anticyclone develops earlier and tends to be stronger throughout the NH summer during La Niña than El Niño. This results in the stronger meridional inflow of ozone-rich air into the NT during La Niña.

Recently, Yan et al. (2018) also showed a later onset of the ASM anticyclone and weaker in-mixing of ozone into the tropics during late boreal spring and early summer (April–June, e.g., AMJ) after boreal winter El Niño events, but they showed almost no difference in the atmospheric circulation and ozone fields during boreal summer (JJA) when compositing on wintertime ENSO index. However, their analysis of three long-lasting El Niño events, which are mainly warm-season ENSO, suggests that El Niño-related ozone anomalies may be stronger and persist longer if El Niño-like conditions are present throughout the summer. This is mainly because the majority of boreal winter ENSO events rapidly decay toward next summer and Niño34 SST anomalies become neutral during JJA (see Figure 3).

Although we only show results from WACCM simulation with coupled oceans, similar results are found for a version of WACCM with prescribed SSTs and a GEOSCCM simulation with coupled ocean. This provides us with additional confidence in results and conclusions made in this study.

The main focus of this study is to understand ozone variability in the tropics and ENSO-related ozone variability outside of the tropics was not examined. However, Figure 4 indicates an increase (decrease) in JJA ozone near 40° N during AMJ El Niño (La Niña) events. A similar ENSO signal in midlatitude ozone during the boreal winter and early spring was previously shown in Calvo et al. (2010), where the higher ozone during El Niño was related to enhanced downwelling branch of the BDC, which transports ozone from the tropics and higher altitudes into midlatitudes and polar regions. Our initial analysis of ozone transport in WACCM (not shown) also indicates strong sensitivity of midlatitude vertical advection in JJA to Niño34 SST anomalies during boreal spring, suggesting that enhanced tropical upwelling and downwelling in the NH midlatitudes is a likely cause of higher ozone in northern midlatitudes during El Niño. However, more work has to be done to quantify

ozone changes in the midlatitudes and polar regions and their relationships to boreal summer ENSO events. These investigations will be the subject of future research.

Another open question is the mechanism by which SSTs in the tropical central-eastern Pacific influences the ASM anticyclone and associated ozone transport into the tropics. One possibility is that the anomalous SSTs in the Pacific lead to changes in the latitudinal position of the Intertropical Convergence Zone over the eastern Indian Ocean and the west Pacific in the preceding spring as well as changes in Walker circulation and Indonesian convection (e.g., Ju & Slingo, 1995), which then modify the onset and strength of the monsoon. But it is also possible the mechanism involves changes in Indian Ocean SSTs (via the *atmospheric bridge* and/or the Indian Ocean dipole) that alter the land-sea contrast and thus the summer monsoon (Cherchi et al., 2007; Lau & Nath, 2000; Song et al., 2007). There is a high correlation between tropical SSTs over the central-eastern Pacific and those over the western Indian Ocean, and the strength of the ASM anticyclone is highly correlated with SSTs in both regions (Figure 12). Further research, and perhaps dedicated simulations with anomalous Pacific or Indian ocean SSTs (e.g., Lau & Nath, 2012), is needed to isolate the processes involved in connecting the Pacific SSTs to the monsoon anticyclone and transport of lower stratosphere ozone into tropics.

This study has shown that ENSO-related variability in the strength of the ASM anticyclone impacts the horizontal advection of ozone in the NT. This ENSO-related variability in the ASM anticyclone could also affect other aspects of the atmospheric transport. Stronger monsoonal flow in the lower stratosphere could potentially lead to stronger ozone intrusions into the troposphere and thus have a significant impact on near-surface climate and amounts of ozone near the surface. Furthermore, previous studies show the important role of ASM as a vertical transport pathway for tropospheric air entering the lower stratosphere (Pan et al., 2016; Park et al., 2007; Randel et al., 2010). An important question is whether or not boreal summer ENSO modifies the time scales of this transport pathway and also the confinement of surface pollutants and tropospheric gases within the anticyclone.

Acknowledgments
This material is based upon work supported by the National Science Foundation Graduate Research Fellowship Program under grant (DGE-1232825), the NASA ACMAP program under grant numbers (NNX15AE48G and NNX17AI31G), and NCAR Advance Study Program (ASP) Graduate Student Visitor Program Fellowship. We would also like to acknowledge and thank all members of the modeling and data science and support teams. M. A. acknowledges funding from the research grant Atraccion de Talento Comunidad de Madrid (ref: 2016-T2/AMB-1405) and the Spanish project STEADY (CGL2017-83198-R). WACCM is a component of the Community Earth System Model (CESM), which is supported by the NSF and the Office of Science of the U.S. Department of Energy. Computing resources were provided by NCAR's Climate Simulation Laboratory, sponsored by the NSF and other agencies. This research was enabled by the computational and storage resources of NCAR's Computational and Information Systems Laboratory (CISL). Authors are thankful to S. E. Strahan and R. S. Stolarski for comments on the paper. MERRA-2 and MLS data are available from the NASA Goddard Space Flight Center Earth Sciences Data and Information Services Center. HadISST data can be obtained from the server at the Hadley Centre in the United Kingdom (https://www.metoffice.gov.uk/hadobs/hadisst/data/download.html). WACCM data are provided via https://www.earthsystemgrid.org/search.html?Project=CCMI1. We thank the two reviewers for their substantive comments that helped to improve the manuscript.

References

Abalos, M., Legras, B., & Shuckburgh, E. (2016). Interannual variability in effective diffusivity in the upper troposphere/lower stratosphere from reanalysis data. *Quarterly Journal of the Royal Meteorological Society*, *142*(697), 1847–1861. https://doi.org/10.1002/qj.2779

Abalos, M., Randel, W., Kinnison, D., & Serrano, E. (2013). Quantifying tracer transport in the tropical lower stratosphere using WACCM. *Atmospheric Chemistry and Physics*, *13*(10), 591–510. https://doi.org/10.5194/acp-13-10591-2013

Andrews, D. G., Holton, J. R., & Leovy, C. B. (1987). *Middle Atmosphere Dynamics*, vol. 40. New York, NY, USA: Academic Press.

Bosilovich, M. G., Akella, S., Coy, L., Cullather, R., Draper, C., Gelaro, R., et al. (2015). MERRA-2: Initial evaluation of the climate, (*NASA Technical Report Series on Global Modeling and Data Assimilation, NASA/TM-2015-104606*). Greenbelt, MD: Goddard Space Flight Center: NASA.

Brönnimann, S., Luterbacher, J., Staehelin, J., Svendby, T. M., Hansen, G., & SvenØ, T. (2004). Extreme climate of the global troposphere and stratosphere 1940–1942 related to El Niño. *Nature*, *431*, 971–974.

Calvo, N., Garcia, R. R., Randel, W. J., & Marsh, D. R. (2010). Dynamical mechanism for the increase in tropical upwelling in the lowermost tropical stratosphere during warm ENSO events. *Journal of the Atmospheric Sciences*, *67*(7), 2331–2340. https://doi.org/10.1175/2010JAS3433.1

Cherchi, A., Gualdi, S., Behera, S., Luo, J. J., Masson, S., Yamagata, T., & Navarra, A. (2007). The influence of tropical Indian Ocean SSTs on the Indian summer monsoon. *Journal of Climate*, *20*(13), 3083–3105. https://doi.org/10.1175/JCLI4161.1

Chowdary, J. S., Harsha, H. S., Gnanaseelan, C., Srinivas, G., Parekh, A., Pillai, P., & Naidu, C. V. (2016). Indian summer monsoon rainfall variability in response to differences in the decay phase of El Niño. *Climate Dynamics*, *48*, 2707–2727. https://doi.org/10.1007/s00382-016-3233-1

Garcia, R. R., Marsh, D., Kinnison, D. E., Boville, B., & Sassi, F. (2007). Simulation of secular trends in the middle atmosphere, 1950-2003. *Journal of Geophysical Research*, *112*, D09301. https://doi.org/10.1029/2006JD007485

Garcia, R. R., Smith, A. K., Kinnison, D. E., de la Cámara, A., & Murphy, D. (2017). Modification of the gravity wave parameterization in the whole atmosphere community climate model: Motivation and results. *Journal of the Atmospheric Sciences*, *74*(1), 275–291. https://doi.org/10.1175/JAS-D-16-0104.1

Garny, H., Bodeker, G. E., & Dameris, M. (2007). Trends and variability in stratospheric mixing: 1979–2005. *Atmospheric Chemistry and Physics*, *7*(3), 6189–6228. https://doi.org/10.5194/acp-7-5611-2007

Gelaro, R., McCartya, W., Suáreza, M. J., Todlinga, R., Moloda, A., Takacsa, L., et al. (2017). The Modern-Era Retrospective Analysis for Research and Applications, version 2 (MERRA-2). *Journal of Climate*, *30*, 5419–5454. https://doi.org/10.1175/JCLI-D-16-0758.1

Intergovernmental Panel on Climate Change (2014). Climate change. Geneva, Switzerland: IPCC.

Jian, R., & Rong-Cai, R. (2014). Atmospheric and oceanic science letters statistical characteristics of ENSO events in CMIP5 models statistical characteristics of ENSO events in CMIP5 models. *Atmospheric and Oceanic Science Letters*, *76*(710), 546–552. https://doi.org/10.3878/AOSL20140055

Ju, J., & Slingo, J. (1995). The Asian summer monsoon and ENSO. *Quarterly Journal of the Royal Meteorological Society*, *121*(525), 1133–1168.

Kim, S. T., & Yu, J. (2012). The two types of ENSO in CMIP5 models. *Geophysical Research Letters*, *39*, L11704. https://doi.org/10.1029/2012GL052006

Konopka, P., Grooß, J.-U., Günther, G., Ploeger, F., Pommrich, R., Müller, R., & Livesey, N. (2010). Annual cycle of ozone at and above the tropical tropopause: Observations versus simulations with the Chemical Lagrangian Model of the Stratosphere (CLaMS). *Atmospheric Chemistry and Physics*, *10*(1), 121–132. https://doi.org/10.5194/acp-10-121-2010

Lau, N. C., & Nath, M. J. (2000). Impact of ENSO on the variability of the Asian-Australian monsoons as simulated in GCM experiments. *Journal of Climate*, *13*(24), 4287–4309. https://doi.org/10.1175/1520-0442(2000)013<4287:IOEOTV>2.0.CO;2

Lau, N. C., & Nath, M. J. (2012). A model study of the air-sea interaction associated with the climatological aspects and interannual variability of the South Asian summer monsoon development. *Journal of Climate*, *25*(3), 839–857. https://doi.org/10.1175/JCLI-D-11-00035.1

Li, Z., Yang, S., Hu, X., Dong, W., & He, B. (2018). Charge in long-lasting El Niño events by convection-induced wind anomalies over the Western Pacific in boreal spring. *Journal of Climate*, *31*, 3755–3763. https://doi.org/10.1175/JCLI-D-17-0558.1

Livesey, N. J., Read, W. G., Wagner, P. A., Froidevaux, L., Lam- bert, A., Manney, G. L., et al. (2015). Version 4.2x Level 2 data quality and description document (*Tech. Rep. JPL D-33509 Rev. B,*): Jet Propulsion Laboratory. http://mls.jpl.nasa.gov

Marsh, D. R., Mills, M. J., Kinnison, D. E., Lamarque, J., Calvo, N., & Polvani, L. M. (2013). Climate change from 1850 to 2005 simulated in CESM1(WACCM). *Journal of Climate*, *26*, 7372–7391. https://doi.org/10.1175/JCLI-D-12-00558.1

Meinshausen, M., Smith, S. J., Calvin, K., Daniel, J. S., Kainuma, M. L. T., Lamarque, J.-F., et al. (2011). The RCP greenhouse gas concentrations and their extensions from 1765 to 2300. *Climatic Change*, *109*, 213. https://https://doi.org/10.1007/s10584-011-0156-z

Oman, L. D., Douglass, A. R., Ziemke, J. R., Rodriguez, J. M., Waugh, D. W., & Nielsen, J. E. (2013). The ozone response to ENSO in aura satellite measurements and a chemistry-climate simulation. *Journal of Geophysical Research: Atmospheres*, *118*, 965–976. https://doi.org/10.1029/2012JD018546

Pan, L. L., Honomichl, S. B., Kinnison, D. E., Abalos, M., Randel, W. J., Bergman, J. W., & Bian, J. (2016). Transport of chemical tracers from the boundary layer to stratosphere associated with the dynamics of the Asian summer monsoon. *Journal of Geophysical Research: Atmospheres*, *121*, 14,159–14,174. https://doi.org/10.1002/2016JD025616

Park, M., Randel, W. J., Gettelman, A., Massie, S. T., & Jiang, J. H. (2007). Transport above the Asian summer monsoon anticyclone inferred from Aura Microwave Limb Sounder tracers. *Journal of Geophysical Research*, *112*, D16309. https://doi.org/10.1029/2006JD008294

Ploeger, F., Konopka, P., Müller, R., Fueglistaler, S., Schmidt, T., Manners, J., et al. (2012). Horizontal transport affecting trace gas seasonality in the tropical tropopause layer (TTL). *Journal of Geophysical Research*, *117*, D09303. https://doi.org/10.1029/2011JD017267

Plumb, R. A. (1996). A "tropical pipe" model of stratospheric transport. *Journal of Geophysical Research*, *101*, 3957. https://doi.org/10.1029/95JD03002

Plumb, R. A. (2006). Tracer interrelationships in the stratosphere. *Reviews of Geophysics*, *45*, RG4005. https://doi.org/10.1029/2005RG000179

Randel, W. J., Garcia, R. R., Calvo, N., & Marsh, D. (2009). ENSO Influence on zonal mean temperature and ozone in the tropical lower stratosphere. *Geophysical Research Letters*, *36*, L15822. https://doi.org/10.1029/2009GL039343

Randel, W. J., Park, M., Emmons, L., Kinnison, D., Bernath, P., Walker, K. A., et al. (2010). Asian monsoon transport of pollution to the stratosphere. *Science*, *328*(5978), 611–613. https://doi.org/10.1126/science.1182274

Randel, W. J., Park, M., Wu, F., & Livesey, N. (2007). A large annual cycle in ozone above the tropical tropopause linked to the Brewer-Dobson circulation. *Journal of the Atmospheric Sciences*, *64*(12), 4479–4488. https://doi.org/10.1175/2007JAS2409.1

Rayner, N. A., Parker, D. E., Horton, E. B., Folland, C. K., Alexander, L. V., Rowell, D. P., et al. (2003). Global analyses of sea surface temperature, sea ice, and night marine air temperature since the late nineteenth century. *Journal of Geophysical Research*, *108*(D14), 4407. https://doi.org/10.1029/2002JD002670

Riese, M., Ploeger, F., Rap, A., Vogel, B., Konopka, P., Dameris, M., & Forster, P. (2012). Impact of uncertainties in atmospheric mixing on simulated UTLS composition and related radiative effects. *Journal of Geophysical Research*, *117*, D16305. https://doi.org/10.1029/2012JD017751

Scott, R. K., Shuckburgh, E. F., Cammas, J.-P., & Legras, B. (2003). Stretching rates and equivalent length near the tropopause. *Journal of Geophysical Research*, *108*(D13), 4394. https://doi.org/10.1029/2002JD002988

Song, Q., Vecchi, G. A., & Rosati, A. J. (2007). Indian ocean variability in the GFDL coupled climate model. *Journal of Climate*, *20*(13), 2895–2916. https://doi.org/10.1175/JCLI4159.1

Stolarski, R. S., Waugh, D. W., Wang, L., Oman, L. D., Douglass, A. R., & Newman, P. A. (2014). Seasonal variation of ozone in the tropical lower stratosphere: Southern tropics are different from northern tropics. *Journal of Geophysical Research: Atmospheres*, *119*, 6196–6206. https://doi.org/10.1002/2013JD021294

Tweedy, O., Waugh, D., Stolarski, R., Oman, L., Randel, W., & Abalos, M. (2017). Hemispheric differences in the annual cycle of tropical lower stratosphere transport and tracers. *Journal of Geophysical Research: Atmospheres*, *122*, 7183–7199. https://doi.org/10.1002/2017JD026482

Webster, P. J., & Yang, S. (1992). Monsoon and ENSO: Selectively interactive systems. *Quarterly Journal of the Royal Meteorological Society*, *118*(507), 877–926. https://doi.org/10.1002/qj.49711850705

Yan, X., Konopka, P., Ploeger, F., Tao, M., Müller, R., Bian, J., & Riese, M. (2018). El Niño Southern Oscillation influence on the Asian summer monsoon anticyclone. *Atmospheric Chemistry and Physics*, *18*, 8079–8096. https://doi.org/10.5194/acp-18-8079-2018

Yang, C., & Giese, B. S. (2013). El niño Southern Oscillation in an ensemble ocean reanalysis and coupled climate models. *Journal of Geophysical Research: Oceans*, *118*, 4052–4071. https://doi.org/10.1002/jgrc.20284